UDC 004.8: 621.39 **doi: 10.32620/aktt.2025.4.12**

Vladimir LUKIN[1], Sergii KRYVENKO[1], Andrii PAVLIUK[2]

[1] *National Aerospace University «Kharkiv Aviation Institute», Kharkiv, Ukraine*
[2] *National Technical University of Ukraine «Igor Sikorsky Kyiv Polytechnic Institute», Kyiv, Ukraine*

VISUALLY LOSSLESS COMPRESSION OF MULTILOOK SAR IMAGES

Synthetic aperture radars (SARs) produce a large amount of remote sensing data useful for numerous applications. SAR image resolution improves, leading to an increased size of acquired images that must be transferred to on-land data processing centers or directly to customers. Then, SAR data compression is required. Nowadays, lossy compression is mostly applied, but it is necessary to control losses to avoid undesired (inappropriate) deterioration of useful information contained in SAR images. In this study, we consider visually lossless compression of multilook SAR images using several lossy compression techniques (including modern coders such as BPG, AVIF, and HEIF) and both conventional and visual quality metrics (including PSNR-HVS-M, HaarPSI, and MS-SSIM). Such metrics and the corresponding distortion invisibility thresholds are employed to achieve the maximum possible compression ratio. We show that, in general, the attained compression ratios are approximately 3 if calculated for 8-bit representation of the images to be compressed. Depending on the visual quality metric used, different coders might produce the largest compression ratio. The considered compression techniques are directly applied to normalized SAR without preliminary variance stabilizing transforms. The images used in the tests have the same speckle characteristics as the real-life images acquired by Sentinel-1 synthetic aperture radar operating in multilook mode, i.e., the speckle is simulated as quasi-Gaussian multiplicative spatially correlated noise. Examples of original and compressed images are presented, demonstrating their very high similarity and practical invisibility of distortions introduced by lossy compression. The obtained results are discussed, and further research directions are proposed. In particular, the use of variance-stabilizing transforms must be considered.

Keywords: *synthetic aperture radar; visually lossless compression; speckled image.*

1. Introduction

1.1. Motivation

Radar remote sensing (RS) is known to be efficient and useful in solving numerous tasks in snow cover mapping [1], ecological monitoring [2], oceanography [3], defense [4], etc. Currently, synthetic aperture radars (SARs) are mostly employed due to their ability to provide high spatial resolution [5]. Improved spatial resolution resulted in a larger number of pixels for the same sensed area. In turn, average image size has greatly increased, and this led to problems with both raw data processing and different operations carried out with formed images especially on-board where available resources for data storage and processing are usually limited [6]. Then, it is reasonable to transfer SAR data to on-land centers of image processing for providing their further processing, storage, and dissemination.

SAR image compression has been of prime interest over, at least, recent 30 years [7-9]. It has been shown that lossless compression applied to SAR images is usually inefficient [10] because images are corrupted by speckle – a noise-like phenomenon having multiplicative nature and typical for coherent imaging [11]. Meanwhile, the inherent presence of speckle in SAR images has impact on all other typical operations of image processing including denoising (despeckling) [12], edge and object detection [13], and lossy compression [14, 15]. Lossy compression of SAR images, similarly to lossy compression of noisy images in general [16], exhibits specific noise filtering effect [14, 15]. This filtering, even under the best settings of a coder, is not as efficient as denoising itself by the best existing filters. Because of this, there are several strategies of SAR image lossy compression where the choice of the best one depends on requirements to SAR image processing and their priority as well as on advantages and drawbacks of these strategies. This fact stimulates considering these strategies and developing each of them.

1.2. State-of-the-art

Below we briefly review four possible strategies considering their positive features and shortcomings. The first strategy is to compress an SAR image in optimal operation point (OOP) [15, 16] where OOP is such a

ISSN 1814-4225 (print)
ISSN 2663-2012 (online)

parameter controlling compression (e.g., quality factor for JPEG) that quality of compressed image is maximally close to the quality of the corresponding noise-free image according to a used quality metric (criterion) and compressed image quality is better than original (noisy, uncompressed) image quality. Possible existence of OOP in SAR lossy compression was, probably, first demonstrated in [17] in 90th of the previous century. There are two positive features of this strategy: 1) a rather large CR is usually provided; 2) it does not require pre-filtering on-board saving time and resources. The negative features are that the quality of compressed image is worse than for other strategies and quality of compressed practically cannot be improved by post-filtering on-land. Another strategy presumes pre-filtering on-board with further lossy compression [15]. Its advantages consist in providing better quality of compressed image than for the previous strategy and producing a rather large CR. The drawback is that efficient despeckling should be carried out on-board and this requires time, memory and computational resources. The third and fourth strategies deal with "careful" compression on-board with further despeckling on-land. The difference in these two strategies is that, for the third strategy, PCC is set in such a way that CR is about two times smaller than for OOP and introduced distortions are visible. Then, post-filtering after decompression is able to improve the image quality but not too much. For the fourth strategy, visually lossless compression [15, 18] is carried out that practically preserves properties of original image and offers good pre-requisites for efficient despeckling after decompression. However, such preservation is reached by the expense of quite small CR.

In this paper, we consider the fourth strategy. Our interest to it stems from the following facts. First, compared to compression techniques considered in [15], novel coders have been proposed recently including better portable graphics (BPG) [19], High Efficiency Image File Format (HEIF) [20], and AV1 Image File Format (AVIF) [21] that are the parts of HEVC video coding. Performance of these novel compression techniques has been recently studied for images corrupted by additive white Gaussian noise [16] and shown to be significantly better than for JPEG. Second, new approaches to assessing visual quality of compressed images have appeared [22, 23]. The importance of visual quality assessment has been stressed. Third, new efficient visual quality metrics have been proposed including MDSI [24], HaarPSI [25], and others. Distortion invisibility thresholds have been determined for some visual quality metrics and high correlation between the best metrics has been demonstrated [26]. The aforementioned recent achievements allow obtaining new insights concerning visually lossless compression of SAR images.

1.3. Objectives and the approach

Our objective is to analyze characteristics of visually lossless compression of SAR images for several compression techniques including aforementioned modern coders (BPG, HEIF, AVIF) and compare them. As a particular case of SAR system, we consider Sentinel-1 [27] that has become very popular and attractive for solving practical tasks [28, 29]. The images used in simulations mimic the properties of multilook data provided by Sentinel-1 in dual-polarization mode, i.e. multiplicative nature of spatially correlated speckle with distribution quite close to Gaussian. In our studies, we use three visual quality metrics, namely, PSNR-HVS-M (https://ponomarenko.info/psnrhvsm.htm) based on DCT, MS-SSIM [30] that exploits several scales in image quality assessment, and HaarPSI [25] that incorporates peculiarities of human attention to image regions while assessing image quality. The reason for using three metrics deals with the fact that, although all three metrics are more adequate than traditional PSNR, they are not perfect anyway. Thus, it is worth making general conclusions based on their joint analysis. Recall here that Spearman rank order correlation coefficient (SROCC) between these metrics and mean opinion score for images corrupted by distortions connected with lossy compression in the database TID2013 is equal to 0.935 for MS-SSIM, 0.961 for PSNR-HVS-M, 0.968 for HaarPSI, whilst SROCC is only 0.914 for PSNR and even less (0.893) for famous SSIM. Therefore, the metrics HaarPSI and PSNR-HVS-M are the "most reliable" in our analysis.

2. Materials and methods of research

For obtaining initial insights on performance of lossy compression for multi-look SAR images, we followed methodology proposed in [31]. Since commonly accepted true (noise-free) SAR images are absent (although there are successful attempts in physical-level simulation of SAR images that correspond to canonical scenes [32]), almost noise-free component images for multispectral Sentinel data [33] are exploited as noise-free basis and then speckle with properties practically identical to properties of speckle in multi-look SAR images is simulated.

Fig. 1 illustrates this methodology. The noise-free image used as the first test image in our experiments is presented in Fig. 1,a. Its noisy version is given in Fig. 1,b. Noisy version of the second test image is represented in Fig. 1,c. As seen, noise is clearly seen in almost all fragments of the images except "black" ones proving multiplicative nature of the simulated speckle which is more intensive in regions with larger mean values.

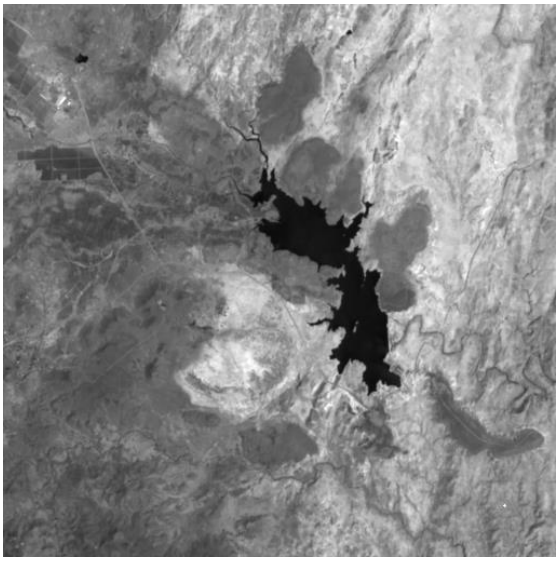

(a)

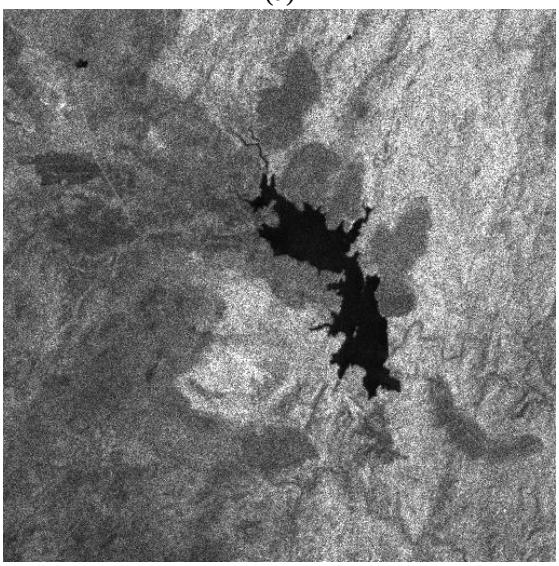

(b)

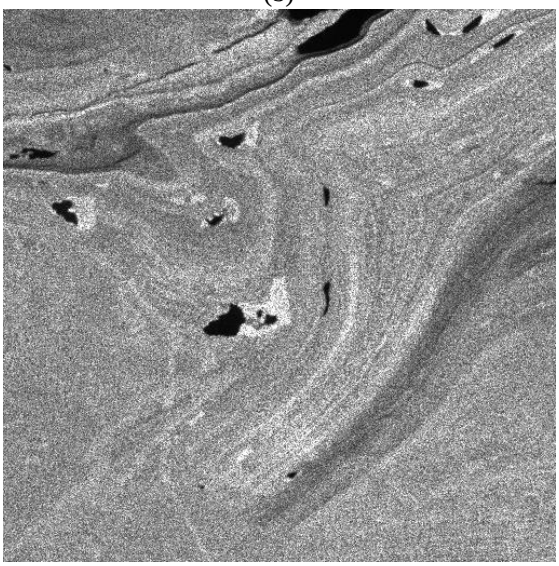

(c)

Fig. 1. Noise-free test image #1 (a), its noisy version (b), and the noisy version of the test image #2

Simultaneously, joint analysis of images in Figures 1,a and 1,b clearly demonstrates how speckle masks low contrast edges and details that can be partly "recovered" by means of efficient denoising.

In our study, we deal with image representation as 8-bit 2D data arrays although more bits (up to 16) are often used for SAR images. There are several reasons behind this. First, some coders (e.g., AGU-M) can be applied only to images presented as 8-bit data arrays. The same holds for some quality metrics. Second, most metrics are designed in such a way that they are "normalized" to the range of image data representation (recall PSNR as one example). Third, distortions introduced by normalization to the range 0-255 and inverse renormalization are usually considerably smaller than distortions that can be introduced by lossy compression in conditions of visually lossless compression. Then, distortions due to normalization operations can be ignored.

In this paper, we consider five coders, namely, JPEG and AGU-M [34] oriented on providing good visual quality by exploiting non-equal quantization of DCT coefficients as well as standard versions of the BPG, HEIF, and AVIF coders. One problem is that these coders use different PCCs that allow varying CR and, respectively, image quality. JPEG, HEIF, and AVIF use quality factors (QFs) that are integers in the limits from 1 (poor quality) to 100 (excellent quality). Note here that AVIF and HEIF have the same compression results for pairs of neighbor PCC values, e.g., 39 and 40. Because of this, we will further consider only odd values of QF. BPG coder uses parameter Q as PCC that varies from 1 to 51 where 1 corresponds to excellent quality and 51 usually relates to poor quality and large CR. AGU-M employs scaling factor (SF) as PCC where SF can be any non-negative value. According to [34], the use of SF about 8, on the average, produces practically invisible distortions.

Typical dependences of PSNR calculated between noisy and compressed images on QF for AVIF and HEIF coders (test image #1) are presented in Fig. 2,a. As seen, they are both monotonously increasing. For small QF, introduced distortions are large (PSNR<25 dB). For large QF (QF>47 dB for HEIF and QF>57 for AVIF), the introduced distortions are small (PSNR>45 dB). Just noticeable difference point # 1 (JND#1) is expected to be in the remained parts of the curves. For the same QF, PSNR values are usually larger for the HEIF coder.

Fig. 2,b presents dependences of CR on QF for the same coders and the same test image. As one can see CR is less than 1.5 for Q≥69 for HEIF and for Q≥93 for AVIF. Then, one deals with near-lossless compression. With QF reduction, CR starts to grow faster. For small QF, the CR growth is very fast.

ISSN 1814-4225 (print)
ISSN 2663-2012 (online)

For approximately equal CR in the area of interest (e.g., CR=6), PSNR for both coders are approximately equal (about 30 dB). Note that here and below CR values are calculated with respect to the 8-bit representation of images to be compressed.

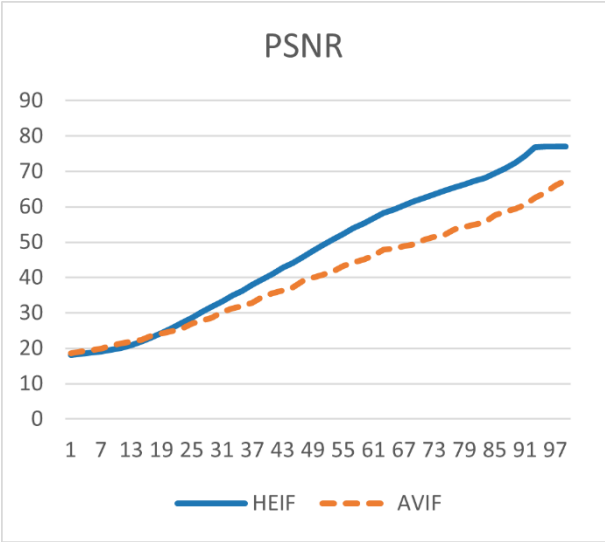

a

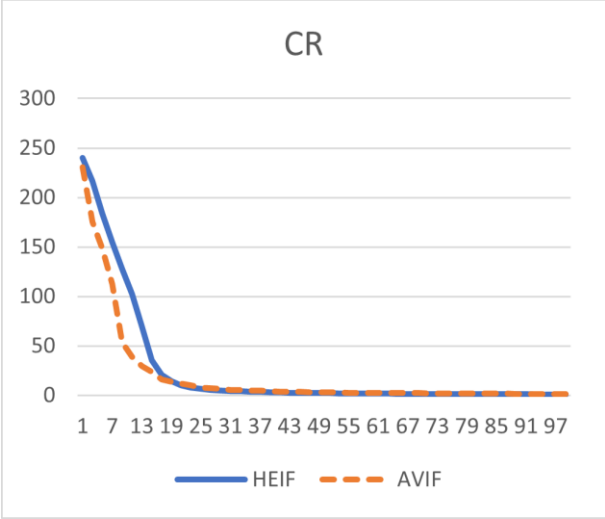

b

Fig. 2. Dependences of PSNR on QF (a) and CR on QF (b) for AVIF and HEIF coders for the test image #1

Concerning visual quality metrics and the corresponding thresholds of distortion invisibility, JND#1, in general, depends on image complexity and noise intensity. However, it is possible to set fixed thresholds that practically guarantee that distortions are invisible. For the considered metrics, this happens [26] if the threshold T is set equal to 0.95 for HaarPSI, 44 dB for PSNR-HVS-M, and 0.99 for MS-SSIM.

Then, having the obtained dependences and setting the corresponding threshold for a considered metric, it is possible to determine all other parameters and metrics. For example, setting the threshold for HaarPSI equal to 0.95, it is possible to approximately determine MSE of introduced distortions, PSNR, CR, PSNR-HVS-M, and MS-SSIM.

One practical question to be discussed here is how to carry out lossy compression with providing a given metric approximately equal to the corresponding threshold. There are two ways to do this: 1) to apply iterative procedures [34] with multiple compression, decompression, metric calculation and PCC changing towards producing metric value close to the threshold; 2) to use the two-step procedure [26] exploiting average rate/distortion curve (RDC), image compression and decompression at the first step and PCC correction and final compression at the second.

3. CR analysis for the Considered Coders

3.1. Examples of RDC

Let us demonstrate examples of RDC for some particular cases. Fig. 3 presents the dependence of HaarPSI on QF for HEIF and AVIF for the test image #2. As seen, both dependences are monotonically increasing. For small QF, difference between images is large (HaarPSI is small). For large QF, images are very similar (HaarPSI is close to unity). Meanwhile, it is easy to determine QS for which the RDCs cross the level 0.95.

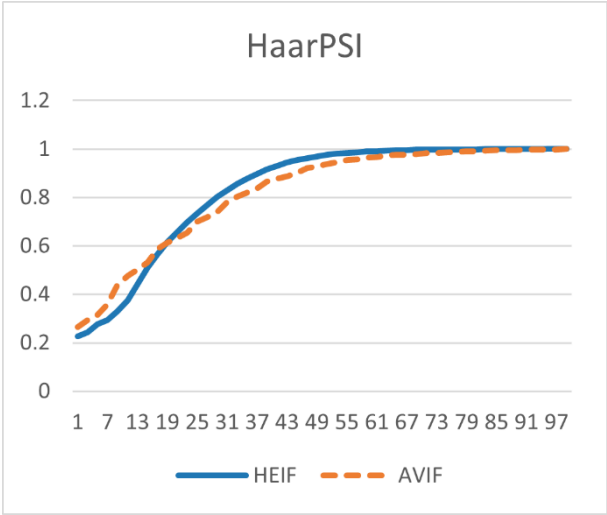

Fig. 3. Dependences of HaarPSI on QF for AVIF and HEIF coders for the test image #2

Fig. 4 represents the RDCs PSNR-HVS-M on Q for the BPG coder for both test images. Very high values of PSNR-HVS-M are observed for Q≤21. Then, with further growth of Q till Q≈45, almost linear decreasing of PSNR-HVS-M with Q growth is observed. After this, RDC behavior is unstable but, according to

PSNR-HVS-M, difference between original and compressed images is significant.

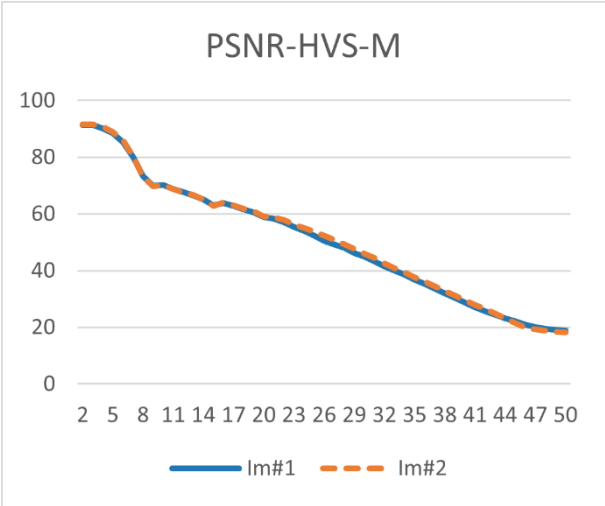

Fig. 4. Dependences of PSNR-HVS-M on Q for the BPG coder for both test images

Finally, Fig. 5 presents the plots of MS-SSIM vs SF for AGU-M for both test images. Although it might seem that the RDCs practically coincide for the considered test images, there is a small difference. The problem of MS-SSIM metric is that its values mainly concentrate in the limits from 0.9 to 1.0.

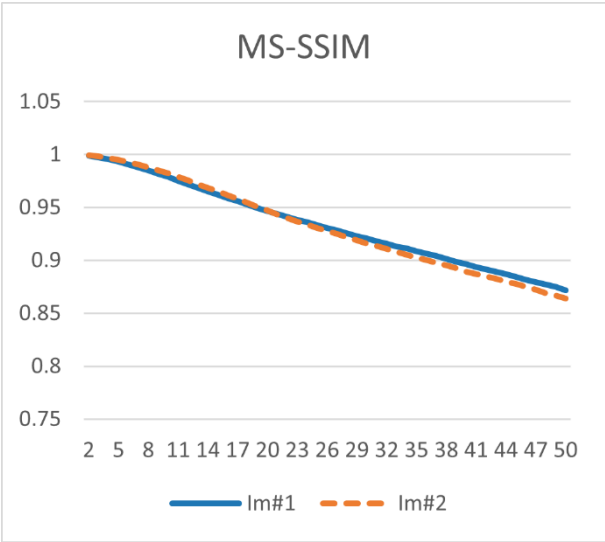

Fig. 5. Dependences of MS-SSIM on SF for the AGU-M coder for both test images

The examples of RDCs given in this subsection show that they are monotonous functions (at least, in the areas of our interest) that allow estimating parameters corresponding to visually lossless compression.

3.2. CR analysis for different threshold settings

Let us now fix the used metric and threshold for it. Let us start from the metric HaarPSI. The obtained data are presented in Table 1. Their analysis shows the following:

1) The desired values of HaarPSI are provided with rather high accuracy that allows comparing the performance characteristics of the coders;

2) The JPEG and AGU-M coders produce considerably larger MSE and, respectively, significantly smaller PSNR than three other coders;

3) MS-SSIM are all about 0.99 or larger showing that introduced distortions are, most probably, invisible; MS-SSIM for the JPEG and AGU-M coders are smaller than for other three coders;

4) Meanwhile, PSNR-HVS-M for the JPEG and AGU-M coders are larger than for other three coders;

5) The results for BPG, HEIF, and AVIF coders are very close to each other;

6) CR in both cases is the largest for AGU-M; visually lossless compression is observed for SF=6;

7) CR for other four coders is slightly smaller than 3.

Consider now the data for the metric PSNR-HVS-M set equal to 44 dB. The obtained data are presented in Table 2. Their analysis demonstrates the following:

1) The JPEG and AGU-M coders again produce considerably larger MSE and smaller PSNR than other four coders;

2) Due to this, they provide CR considerably larger than other three coders;

3) Meanwhile, AGU-M and, especially, JPEG coders produce MS-SSIM and HaarPSI smaller than the corresponding thresholds;

4) The HEIF, BPG, and AVIG coders again produce very similar results and CR for them is smaller than 3.

Finally, let us analyze data for the case of MS-SSIM setting equal to 0.99. These data are collected in Table 3. Their analysis allows concluding the following:

1) Again, MSE for JPEG and AGU-M is larger and PSNR is smaller than for other three coders;

2) PSNR-HVS-M for the JPEG and AGU-M is considerably larger than for other three coders;

3) HaarPSI for the JPEG and AGU-M is also better for the JPEG and AGU-M than for BPG, HEIF, and AVIF although AVIF for JPEG and AGU-M is slightly smaller than for the desired threshold;

4) CR values are mostly slightly smaller than 3 except the data for JPEG;

5) The results for the BPG, HEIF, and AVIF coders are again almost identical.

ISSN 1814-4225 (print)
ISSN 2663-2012 (online)

Table 1

Compression characteristics for using the metric HaarPSI with T=0.95

Image 1						
Coder	CR/PCC	PSNR-HVS-M	MSE	PSNR	MS-SSIM	HaarPSI
JPEG	2.79/72	52.0	110.1	27.7	0.990	0.951
AGU-M	3.42/6	46.40	118.4	27.4	0.991	0.948
BPG	2.73/31	43.29	21.5	34.8	0.995	0.950
HEIF	2.62/45	44.15	19.8	35.2	0.996	0.954
AVIF	2.78/55	43.30	22.2	34.7	0.995	0.948
Image 2						
JPEG	2.60/70	51.6	131.4	26.9	0.992	0.949
AGU-M	3.08/6	47.5	127.0	27.1	0.993	0.952
BPG	2.45/31	44.4	21.5	34.8	0.996	0.955
HEIF	2.44/45	44.3	21.7	34.8	0.996	0.954
AVIF	2.52/55	44.6	21.7	34.8	0.996	0.954

Table 2

Compression characteristics for using the metric PSNR-HVS-M with T=44 dB

Image 1						
Coder	CR/PCC	PSNR-HVS-M	MSE	PSNR	MS-SSIM	HaarPSI
JPEG	4.44/43	43.89	326.2	23.0	0.969	0.864
AGU-M	3.76/7	44.30	152.9	26.3	0.987	0.934
BPG	2.73/31	43.29	21.5	34.8	0.995	0.950
HEIF	2.49/47	45.80	15.7	36.2	0.997	0.962
AVIF	2.69/57	44.26	19.5	35.2	0.996	0.955
Image 2						
JPEG	4.19/38	44.0	462.6	21.4	0.967	0.846
AGU-M	3.62/8	43.2	211.6	24.9	0.988	0.923
BPG	2.45/31	44.4	21.5	34.8	0.996	0.955
HEIF	2.44/45	44.3	21.7	34.8	0.996	0.954
AVIF	2.52/55	44.6	21.7	34.8	0.996	0.954

Table 3

Compression characteristics for using the metric MS-SSIM with T=0.99

Image 1						
Coder	CR/PCC	PSNR-HVS-M	MSE	PSNR	MS-SSIM	HaarPSI
JPEG	2.79/72	52.0	110.1	27.7	0.990	0.951
AGU-M	3.42/6	46.4	118.4	27.3	0.991	0.948
BPG	3.34/34	38.6	44.1	31.7	0.990	0.910
HEIF	3.43/37	37.9	50.2	31.1	0.990	0.901
AVIF	3.31/47	39.0	41.7	31.9	0.991	0.913
Image 2						
JPEG	2.73/67	50.7	158.0	26.1	0.990	0.939
AGU-M	3.34/7	45.1	168.4	25.8	0.990	0.938
BPG	3.16/35	37.7	56.7	30.6	0.990	0.898
HEIF	3.11/37	37.6	56.3	30.6	0.990	0.898
AVIF	3.32/43	37.1	62.5	30.2	0.989	0.888

As one can see, some conclusions coincide for data in all three Tables. In particular, the results for the BPG, HEIF, and AVIF coders are very similar, and they are, in general, not better than for JPEG and AGU-M coders. We associate this with the fact that JPEG and AGU-M are adapted to providing higher visual quality. Meanwhile, the conclusions that follow from the use of different metrics do not fully coincide.

The obtained data have, at least, resulted in initial insights on what PCC to set for the considered coders: QF≈60 for JPEG, SF≈6.5 for AGU-M, Q≈32 for BPG, QF≈43 for HEIF, and QF≈51 for AVIF. Meanwhile, it might be so that PCC depends on image content. Then, more test images are needed for analysis.

It might happen that, according to one metric one coder is better whilst, according to another metric, another coder is the best. As an example, consider the first test image compressed with CR≈3.

The corresponding data are given in Table 4. According to MSE and PSNR, the best results are provided by AVIF and HEIF; according to PSNR-HVS-M, the best are the JPEG and AGU-M coders; according to HaarPSI, AGU-M is the best; and, finally, according to MS-SSIM, four modern coders produced similar results outperforming JPEG.

Table 4

Compression characteristics for CR=3 for the test image #1

Image 1						
Coder	CR/PCC	PSNR-HVS-M	MSE	PSNR	MS-SSIM	HaarPSI
JPEG	2.99/68	50.7	139.1	26.7	0.987	0.940
AGU-M	3.09/5	49.1	86.0	28.78	0.993	0.962
BPG	3.10/33	40.1	34.54	32.75	0.992	0.926
HEIF	2.97/41	40.9	31.59	33.13	0.993	0.931
AVIF	3.07/51	40.8	31.92	33.09	0.993	0.930

One more conclusion is that if one provides CR about 3 (with respect to 8-bit data representation), this practically guarantees that visually lossless compression is ensured. Let us check this hypothesis.

4. Compression Examples and Discussion

4.1. Compression Examples

Fig. 6 presents the compressed images for the coders JPEG, AGU-M, and BPG for the test image #1 where PCC are set according to data in Table 4 to provide CR≈3 for all coders. As seen, the images seem identical and they look the same as the image in Fig. 1,b. No speckle suppression and/or edge/detail/texture smearing are observed.

Fig. 7 demonstrates the compressed images for the HEIF and AVIF coders, the test image and the provided CR are the same as in Fig. 6. The images seem identical to each other, identical to images in Fig. 6, and the same as in Fig. 1,b. This means that visually lossless compression is attained for all coders although images in Figures 6 and 7 have different values of PSNR, PSNR-HVS-M, MS-SSIM, and HaarPSI (see Table 4). This phenomenon might seem strange, but it has two explanations.

4.2. Discussion

The first reason for invisibility of distortions is that, if coders are applied to SAR images directly, essential speckle suppression for small CR takes place in image homogeneous regions with low mean intensity ("black areas") where speckle, due to its low intensity, is practically not seen even in original images (consider "dark" regions in images in Figures 1,b and 1,c. To prove this, Figure 8 and 9 present images compressed by the BPG coder with Q=38 and Q=43. In this case (see the plots in Fig. 4), the introduced distortions should be visible (PSNR-HVS-M<44 dB) and this is really so (compare the images in Figures 8 and 9 to the image in Fig. 6,c). Note that noise filtering effect simultaneously with detail smearing and compression artifacts are mainly observed in relatively dark image areas whilst image quality in brighter regions is still satisfactory (distortions in them are practically invisible). Moreover, distortions for Q=43 are significantly more intensive than for Q=38.

The second reason is that MSE of introduced distortions in all considered cases is smaller than equivalent noise variance in original images. Really, equivalent noise variance σ_{eq}^2 for the images with speckle is approximately equal to $\sigma_\mu^2 \sum_{k=1}^{K} \sum_{l=1}^{L} I_{t\,kl}^2 / KL$ where σ_μ^2 denotes the speckle relative variance (approximately equal to 0.05 for multi-look images that we consider), K and L define the image size and $I_{t\,kl}^2$ is the true image value in a kl-th pixel. For SAR images represented as 8-bit data $\sum_{k=1}^{K} \sum_{l=1}^{L} I_{t\,kl}^2 / KL$ is about 10000 or larger, and, thus, σ_{eq}^2 is about 500 or larger. Then, even in the worst cases (see data for JPEG in Tables 1 and 4), MSE of introduced losses is several times smaller than σ_{eq}^2.

CR about 3 is not large. On the one hand, the obtained CR values are at the same level as in [15]. On the other hand, the attained CR might be unsatisfactory for practice. The results presented in [15] show that visually lossless compression can be also reached using variance stabilizing transform of logarithmic/exponential type with providing larger CR values. Logarithmic type transform is applied before lossy compression and inverse exponential transform is applied after decompression. The use of such transforms slightly complicates processing, but they are very fast. Therefore, it is worth studying this approach in the future.

5. Conclusions

Visually lossless compression of multilook SAR images is considered. It is demonstrated that attained compression ratios (compared to images represented as 8-bit data arrays) are about 3. Three visual quality metrics with the corresponding distortion invisibility thresholds have been analyzed and as shown, the results are slightly different - different coders might produce the largest compression ratio and/or the best quality. Examples demonstrating that original and compressed images are practically identical are presented. The results obtained for two test SAR images are discussed.

The directions of research to be conducted in the future are considered. In particular, the use of variance stabilizing transforms should be studied.

ISSN 1814-4225 (print)
ISSN 2663-2012 (online)

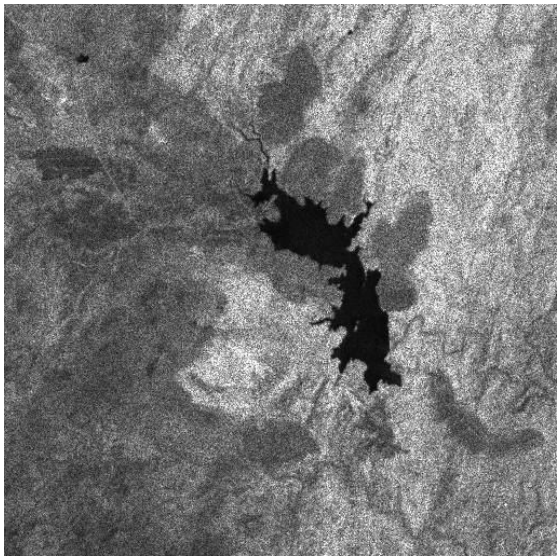

a

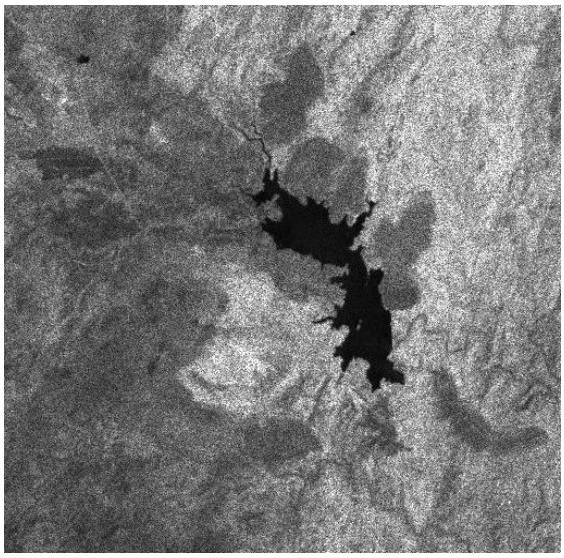

b

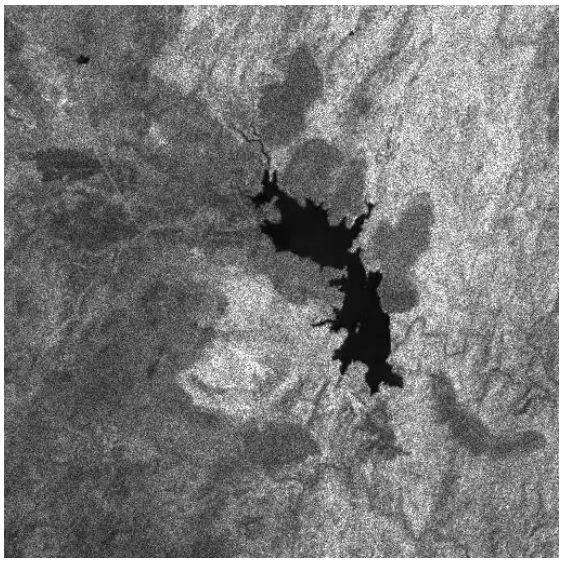

c

Fig. 6. Compressed noisy test image #1 using the JPEG (a), AGU-M (b), and BPG (c) coders with providing CR≈3

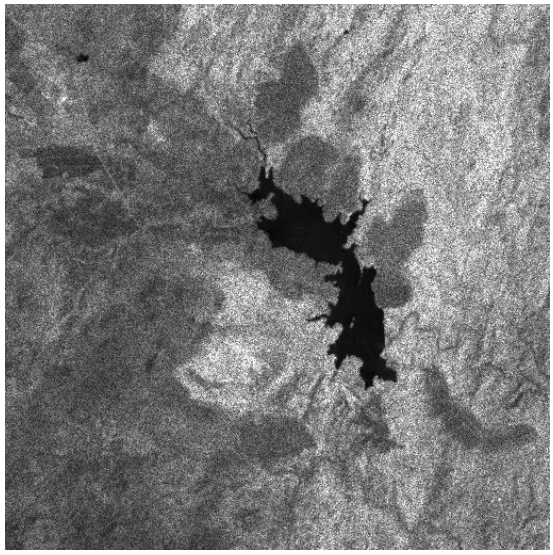

a

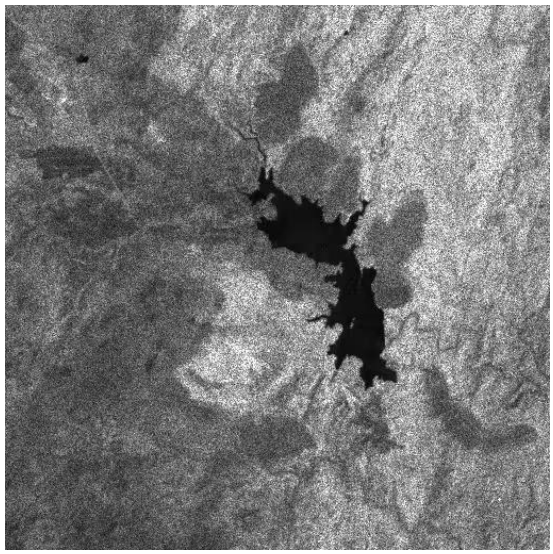

b

Fig. 7. Compressed noisy test image #1 using the HEIF (a) and AVIF (b) coders with providing CR≈3

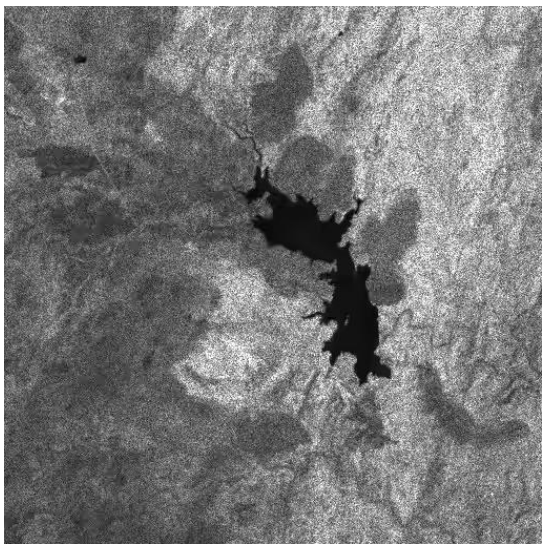

Fig. 8. Compressed noisy test image #1 using the BPG with Q=38

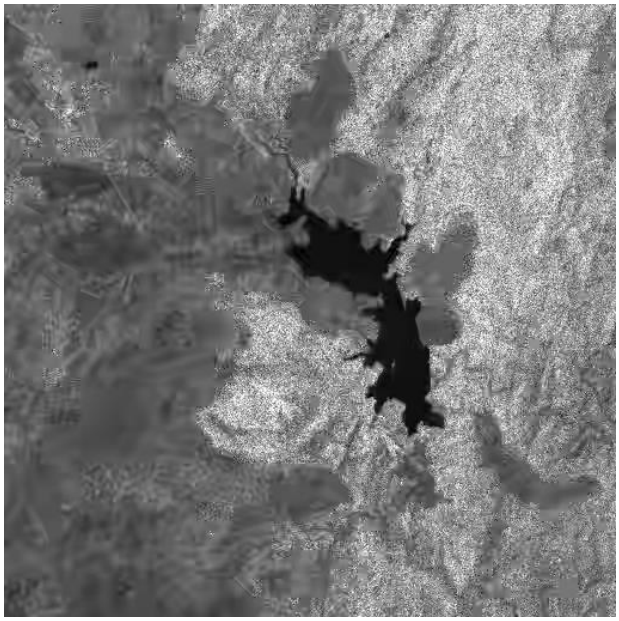

Fig. 9. Compressed noisy test image #1
using the BPG with Q=43

Contributions of authors: conception – **Vladimir Lukin**; methodology – **Vladimir Lukin**; problem formulation – **Vladimir Lukin**; analysis – **Andrii Pavliuk, Sergii Kryvenko**; model development – **Andrii Panliuk**; software – **Sergii Kryvenko**; validation – **Vladimir Lukin**, **Sergii Kryvenko**; analysis of results – **Andrii Pavliuk**; visualization –**Andrii Pavliuk**; writing – **Sergii Kryvenko**; revision and editing – **Vladimir Lukin**, **Sergii Kryvenko, Andrii Pavliuk**.

Conflict of interest

The authors declare that they have no conflict of interest in relation to this research, whether financial, personal, authorship, or otherwise, that could affect the research and its results presented in this paper.

Financing

The research has been funded by National Research Foundation of Ukraine (https://nrfu.org.ua/en/, accessed on 1 July 2025) within Project No. 2023. 04/0039 "Geospatial monitoring system for the war impact on the agriculture of Ukraine based on satellite data" (2024-2025).

Use of Artificial Intelligence

The authors confirm that they did not use artificial intelligence technologies when creating the current work.

All authors have read and agreed to the published version of this manuscript.

References

1. Varade, D., Singh, G., Dikshit, O., & Manickam, S. Identification of Snow Using Fully Polarimetric SAR Data Based On Entropy and Anisotropy. *Water Resources Research*, 2020, vol. 56, pp. 1–18. DOI: 10.1029/2019WR025449.

2. Lysenko, A. SAR Data Spatial Resolution Enhancement for Environmental Monitoring Tasks. *International Conference of Young Professionals «GeoTerrace-2023»,* Oct 2023, Volume 2023, iss. 1, pp. 1–5. DOI: 10.3997/2214-4609.2023510010.

3. Asiyabi, R. M., Ghorbanian, A., Tameh, S. N., Amani, M., Jin, S., & Mohammadzadeh, A. Synthetic Aperture Radar (SAR) for Ocean: A Review. *IEEE Journal of Selected Topics in Applied Earth Observations and Remote Sensing*, 2023, vol. 16, pp. 9106–9138. DOI. 10.1109/JSTARS.2023.3310363.

4. Gao, W., Liu, Y., Zeng, Y., Liu, Q., & Li, Q. (2023). SAR Image Ship Target Detection Adversarial Attack and Defence Generalization Research. *Sensors*, 2023, vol. 23, iss. 4. DOI: 10.3390/s23042266.

5. Okada, Y., Nakamura, S., Iribe, K., Yokota, Y., Tsuji, M., Tsuchida, M., Hariu, K., Kankaku, Y., Suzuki, S., Osawa, Y., & Shimada, M. System design of wide swath, high resolution, full polarimietoric L-band SAR onboard ALOS-2. *2013 IEEE International Geoscience and Remote Sensing Symposium - IGARSS*, 2013, pp. 2408–2411. DOI: 10.1109/IGARSS.2013.6723305.

6. Breit, H., Wiehle, S., Mandapati, S., Günzel, D., & Balss, U. Demonstrating a SAR Satellite Onboard Processing Chain. *7th Workshop on RF and Microwave Systems, Instruments & Sub-systems + 5th Ka-band Workshop,* 2022, pp. 1-6. Available at: https://elib.dlr.de/188283/1/SO6P1P_DLR_Demonstrating_a_SAR_Satellite_Onboard_Processing-Breit-Helko.pdf (accessed 12.6.2024).

7. Datcu, M., Schwarz, G., Schmidt, K., & Reck, C. Quality Evaluation of Compressed Optical and SAR Images: JPEG vs. Wavelets. Proc. of *1995 International Geoscience and Remote Sensing Symposium, IGARSS '95*, Florence, Italy, 10-14 July 1995, pp. 1687–1689. Available at: https://elib.dlr.de/23745/(accessed 12.6.2024).

8. Kozhemiakin, R., Abramov, S., Lukin, V., Djurović, B., Djurović, I., & Simeunović, M. Strategies of SAR image lossy compression by JPEG2000 and SPIHT. *2017 6th Mediterranean Conference on Embedded Computing (MECO)*, 2017, pp. 1–6. DOI: 10.1109/MECO.2017.7977176.

9. Deng, J., & Huang, L. Synthetic Aperture Radar Image Compression Based on Low-Frequency Rejection and Quality Map Guidance. *Remote Sensing,* 2024, vol. 16, iss. 5, article on. 891. DOI: 10.3390/rs16050891.

10. Rusyn, B., Lutsyk, O., Lysak, Y., Lukenyuk, A., & Pohreliuk, L. Lossless image compression in the remote sensing applications. *2016 IEEE First International Conference on Data Stream Mining & Processing (DSMP)*, Lviv, Ukraine, 2016, pp. 195–198. DOI: 10.1109/DSMP.2016.7583539.

ISSN 1814-4225 (print)
ISSN 2663-2012 (online)

11. Yin, D., Gu, Z., Zhang, Y., Gu, F., Nie, S., Feng, S., Ma, J., & Yuan, C. Speckle noise reduction in coherent imaging based on deep learning without clean data. *Optics and Lasers in Engineering*, 2020, vol. 133, article no. 106151. DOI: 10.1016/j.optlaseng.2020.106151.

12. Ko, J., & Lee, S. SAR Image Despeckling Using Continuous Attention Module. *IEEE Journal of Selected Topics in Applied Earth Observations and Remote Sensing,* 2020, vol. 15, pp. 3–19. DOI: 10.1109/JSTARS.2021.3132027.

13. Sun, Z., Leng, X., Zhang, M., Ren, H., & Ji, K. SAR Image Object Detection and Information Extraction: Methods and Applications. *Remote Sensing*, 2025, vol. 17, iss. 12, article no. 2098. DOI: 10.3390/rs17122098.

14. Liu, Z., Wang, S., & Gu, Y. SAR Image Compression with Inherent Denoising Capability Through Knowledge Distillation. *IEEE Geoscience and Remote Sensing Letters*, 2024, vol. 21, article no. 4008005, pp. 1–5. DOI: 10.1109/LGRS.2024.3386758.

15. Ponomarenko, N. N., Lukin, V. V., Kozhemiakin, R. A., Egiazarian, K. O., & Chobanu, M. K. Lossy and visually lossless compression of single-look SAR images. *Telecommunications and Radio Engineering*, 2013, vol. 72, iss. 8, pp. 711–729. DOI: 10.1615/TelecomRadEng.v72.i8.60.

16. Kryvenko, S., Lukin, V., & Vozel, B. Lossy Compression of Single-channel Noisy Images by Modern Coders. *Remote Sensing*, 2024, vol. 16, iss. 12, article no. 2093. DOI: 10.3390/rs16122093.

17. Odegard, J. E., Guo, H., Lang, M., Burrus, C. S., Jr., R. O. W., Novak, L. M., & Hiett, M. Wavelet-based SAR speckle reduction and image compression. In *Algorithms for Synthetic Aperture Radar Imagery II*, 1995, vol. 2487, pp. 259–271. SPIE. DOI: 10.1117/12.210843.

18. Bondzulic, B., Pavlović, B., Stojanovic, N., & Petrovic, V. Picture-wise just noticeable difference prediction model for JPEG image quality assessment. *Military Technical Courier,* 2022, vol. 70, pp. 62–86. DOI: 10.5937/vojtehg70-34739.

19. Yee, D., Soltaninejad, S., Hazarika, D., Mbuyi, G., Barnwal, R., & Basu, A. Medical image compression based on region of interest using better portable graphics (BPG). *2017 IEEE International Conference on Systems, Man, and Cybernetics (SMC)*, Banff, AB, Canada, 2017, pp. 216–221. DOI: 10.1109/SMC.2017.8122605.

20. Lainema, J., Hannuksela, M., Malamal Vadakital, V., & Aksu, E. HEVC still image coding and high efficiency image file format. *2016 IEEE International Conference on Image Processing (ICIP)*, Phoenix, AZ, USA, 2016, pp. 71-75. DOI: 10.1109/ICIP.2016.7532321.

21. Chen, Y., Mukherjee, D., Han, J., Grange, A., Xu, Y., Parker, S., Chen, C., Su, H., Joshi, U., Chiang, C.-H., Wang, Y., Wilkins, P., Bankoski, J., Trudeau, L., Egge, N., Valin, J.-M., Davies, T., Midtskogen, S., Norkin, A., & Liu, Z. An Overview of Coding Tools in AV1: the First Video Codec from the Alliance for Open Media. *APSIPA Transactions on Signal and Information Processing*, 2020, vol. 9, iss. 1, article no. e6. DOI: 10.1017/ATSIP.2020.2.

22. Testolina, M., Lazzarotto, D., Rodrigues, R., Mohammadi, S., Ascenso, J., Pinheiro, A., & Ebrahimi, T. On the Performance of Subjective Visual Quality Assessment Protocols for Nearly Visually Lossless Image Compression. *MM '23: Proceedings of the 31st ACM International Conference on Multimedia,* 2023, pp. 6715–6723. DOI: 10.1145/3581783.3613835.

23. Jamil, S. Review of Image Quality Assessment Methods for Compressed Images. *Journal of Imaging*, 2024, vol. 10, iss. 5, article no. 113. DOI: 10.3390/jimaging10050113.

24. Nafchi, H., Shahkolaei, A., Hedjam, R., & Cheriet, M. Mean Deviation Similarity Index: Efficient and Reliable Full-Reference Image Quality Evaluator. *IEEE Access*, 2016, vol. 4, pp. 5579–5590. DOI: 10.1109/ACCESS.2016.2604042.

25. Reisenhofer, R., Bosse, S., Kutyniok, G., & Wiegand, T. A Haar Wavelet-Based Perceptual Similarity Index for Image Quality Assessment. *Signal Processing Image Communication*, 2018, vol. 61, pp. 33–43. DOI: 10.1016/j.image.2017.11.001.

26. Li, F., Ieremeiev, O., Lukin, V., & Egiazarian, K. BPG-Based Lossy Compression of Three-Channel Remote Sensing Images with Visual Quality Control. *Remote Sensing*, 2024, vol. 16, iss. 15, article no. 2740. DOI: 10.3390/rs16152740.

27. *Sentinel-1 - Sentinel Online*. Available at: https://sentinels.copernicus.eu/copernicus/sentinel-1. (accessed 12.6.2024).

28. Abdikan, S., Balik Sanli, F., Ustuner, M., & Calò, F. Land Cover Mapping Using SENTINEL-1 SAR Data. *ISPRS - International Archives of the Photogrammetry, Remote Sensing and Spatial Information Sciences,* XLI-B7, 2016, pp. 757–761. DOI: 10.5194/isprs-archives-XLI-B7-757-2016.

29. Fan, D., Zhao, T., Jiang, X., García-García, A., Schmidt, T., Samaniego, L., Attinger, S., Wu, H., Jiang, Y., Shi, J., Fan, L., Tang, B.-H., Wagner, W., Dorigo, W., Gruber, A., Mattia, F., Balenzano, A., Brocca, L., Jagdhuber, T., …, & Peng, J. A Sentinel-1 SAR-based global 1-km resolution soil moisture data product: Algorithm and preliminary assessment. *Remote Sensing of Environment,* 2025, vol. 318, article no. 114579. DOI: 10.1016/j.rse.2024.114579.

30. Wang, Z., Bovik, A. C., Sheikh, H. R., & Simoncelli, E. P. Image quality assessment: from error visibility to structural similarity. *IEEE Transactions on Image Processing*, 2004, vol. 13, iss. 4, pp. 600–612. DOI: 10.1109/TIP.2003.819861.

31. Rubel, O., Lukin, V., Rubel, A., & Egiazarian, K. Selection of Lee Filter Window Size Based on Despeckling Efficiency Prediction for Sentinel SAR Images. *Remote Sensing,* 2021, vol. 13, iss. 10. DOI: 10.3390/rs13101887.

32. Di Martino, G., Poderico, M., Poggi, G., Riccio, D., & Verdoliva, L. SAR image simulation for the assessment of despeckling techniques. *2012 IEEE International Geoscience and Remote Sensing*

Symposium, 2012, pp. 1797–1800. DOI: 10.1109/IGARSS.2012.6351163.

33. De Fioravante, P., Luti, T., Cavalli, A., Giuliani, C., Dichicco, P., Marchetti, M., Chirici, G., Congedo, L., & Munafò, M. (2021). Multispectral Sentinel-2 and SAR Sentinel-1 Integration for Automatic Land Cover Classification. *Land,* 2021, vol. 10, iss. 6, article no. 611. DOI: 10.3390/land10060611.

34. Zemliachenko, A. N., Lukin, V. V., Ponomarenko, N. N., Egiazarian, K. O., & Astola, J. Still image/video frame lossy compression providing a desired visual quality. *Multidimens. Syst. Signal Process*, 2016, vol. 27, iss. 3, pp. 697–718. DOI: 10.1007/s11045-015-0333-8.

Надійшла до редакції 10.05.2025, розглянута на редколегії 18.08.2025

ВІЗУАЛЬНО БЕЗВТРАТНЕ СТИСНЕННЯ БАГАТОВИГЛЯДОВИХ РСА-ЗОБРАЖЕНЬ

В. В. Лукін, С. С. Кривенко, А. Д. Павлюк

Радари із синтезованою апертурою (РСА) створюють велику кількість даних дистанційного зондування, корисних для численних застосувань. Роздільна здатність зображень РСА покращується, що призводить до збільшення розміру отриманих зображень, які необхідно передавати до наземних центрів обробки даних або безпосередньо користувачам. Тоді потрібне стиснення даних РСА. В даний час переважно застосовується стиснення з втратами, але необхідно контролювати втрати, щоб уникнути небажаного (неналежного) погіршення корисної інформації, що міститься в РСА-зображеннях. У цій статті ми розглядаємо візуально безвтратне стиснення багатопогляжових РСА-зображень з використанням кількох методів стиснення з втратами (включаючи такі сучасні кодери, як BPG, AVIF та HEIF) та як звичайних, так і візуальних метрик якості (включаючи PSNR-HVS-M, HaarPSI та MS-SSIM). Такі метрики та відповідні пороги невидимості спотворень використовуються для досягнення максимально можливого коефіцієнта стиснення. Показано, що загалом досягнуті коефіцієнти стиснення становлять близько 3, якщо розраховувати їх відносно 8-бітного представлення зображень, що стискаються. Залежно від використовуваної метрики візуальної якості, різні кодери можуть досягати найбільшого коефіцієнта стиснення. Розглянуті методи стиснення застосовуються безпосередньо до нормованого РСА-зображення, без попередніх варіаційно-стабілізуючих перетворень. Зображення, що використовуються в тестах, мають ті ж характеристики спеклу, що й реальні зображення, отримані РСА Sentinel-1, що працює в багатопоглядовому режимі, тобто спекл моделюється як квазігауссівський мультиплікативний просторово корельований шум. Представлено приклади оригінальних та стиснутих зображень, що демонструють їх дуже високу подібність та практичну невидимість спотворень, внесених стисненням з втратами. Обговорюються отримані результати та пропонуються напрямки подальших досліджень. Зокрема, необхідно розглянути використання варіаційно-стабілізуючих перетворень.

Ключові слова: радар з синтезованою апертурою; візуально безвтратне стиснення; спекл; зображення.

Лукін Володимир Васильович – д-р техн. наук, проф., зав. каф. інформаційно-комунікаційних технологій ім. О. О. Зеленського, Національний аерокосмічний університет «Харківський авіаційний інститут», Харків, Україна.

Кривенко Сергій Станіславович – канд. техн. наук, докторант каф. інформаційно-комунікаційних технологій ім. О. О. Зеленського, Національний аерокосмічний університет «Харківський авіаційний інститут», Харків, Україна.

Павлюк Андрій Дмитрович – ас. каф. мат. моделювання та аналізу даних, Національний технічний університет України «Київський політехнічний інститут імені Ігоря Сікорського», Київ, Україна.

Vladimir Lukin – Doctor of Technical Sciences, Professor, Head of the Department of Information and Communication Technologies named after O. O. Zelensky, National Aerospace University "Kharkiv Aviation Institute", Kharkiv, Ukraine,
e-mail: v.lukin@khai.edu, ORCID: 0000-0002-1443-9685.

Sergii Kryvenko – Candidate of Technical Science, Doctorate Student of the Department of Information and Communication Technologies named after O. O. Zelensky, National Aerospace University "Kharkiv Aviation Institute", Kharkiv, Ukraine,
e-mail: s.kryvevnko@khai.edu, ORCID: 0000-0001-6027-5442.

Andrii Pavliuk – Assistant at the Department of Mathematical Modeling and Data Analysis, National Technical University of Ukraine «Igor Sikorsky Kyiv Polytechnic Institute», Kyiv, Ukraine
e-mail: andpa-ipt21@lll.kpi.ua, ORCID: 0009-0002-7283-6360.